Geminal embedding scheme for optimal atomic basis set construction in correlated calculations

S. Sorella, N. Devaux, M. Dagrada, G. Mazzola, and M. Casula

Citation: The Journal of Chemical Physics **143**, 244112 (2015); doi: 10.1063/1.4938089

View online: http://dx.doi.org/10.1063/1.4938089

View Table of Contents: http://aip.scitation.org/toc/jcp/143/24

Published by the American Institute of Physics

Geminal embedding scheme for optimal atomic basis set construction in correlated calculations

S. Sorella,[1,a)] N. Devaux,[2] M. Dagrada,[2,b)] G. Mazzola,[3,c)] and M. Casula[4,d)]
[1]*International School for Advanced Studies (SISSA), Via Beirut 2-4, 34014 Trieste, Italy and INFM Democritos National Simulation Center, Trieste, Italy*
[2]*Institut de Minéralogie, de Physique des Matériaux et de Cosmochimie, Université Pierre et Marie Curie, Case 115, 4 Place Jussieu, 75252 Paris Cedex 05, France*
[3]*Theoretische Physik, ETH Zurich, 8093 Zurich, Switzerland*
[4]*CNRS and Institut de Minéralogie, de Physique des Matériaux et de Cosmochimie, Université Pierre et Marie Curie, Case 115, 4 Place Jussieu, 75252 Paris Cedex 05, France*

(Received 18 May 2015; accepted 3 December 2015; published online 28 December 2015)

We introduce an efficient method to construct optimal and system adaptive basis sets for use in electronic structure and quantum Monte Carlo calculations. The method is based on an embedding scheme in which a reference atom is singled out from its environment, while the entire system (atom and environment) is described by a Slater determinant or its antisymmetrized geminal power (AGP) extension. The embedding procedure described here allows for the systematic and consistent contraction of the primitive basis set into geminal embedded orbitals (GEOs), with a dramatic reduction of the number of variational parameters necessary to represent the many-body wave function, for a chosen target accuracy. Within the variational Monte Carlo method, the Slater or AGP part is determined by a variational minimization of the energy of the whole system in presence of a flexible and accurate Jastrow factor, representing most of the dynamical electronic correlation. The resulting GEO basis set opens the way for a fully controlled optimization of many-body wave functions in electronic structure calculation of bulk materials, namely, containing a large number of electrons and atoms. We present applications on the water molecule, the volume collapse transition in cerium, and the high-pressure liquid hydrogen. © *2015 AIP Publishing LLC.* [http://dx.doi.org/10.1063/1.4938089]

I. INTRODUCTION

In *ab initio* quantum chemistry and computational condensed matter physics, the optimization of the basis set has been, just from the very beginning, a crucial ingredient for defining feasible algorithms that can provide meaningful and converged physical and chemical properties in electronic calculations.

In density functional theory (DFT) calculations with periodic boundary conditions, plane-wave (PW) basis sets are mostly used since their systematic convergence can be controlled by just a single parameter, the PW cutoff. This outweighs disadvantages such as the loss of a chemical intuitive picture, and the need of pseudopotentials to smooth out the core region. On the other hand, large-scale coarse-graining or $O(N)$ — N being the total number of electrons— algorithms typically require localized basis sets.[1]

In quantum chemistry calculations, mainly based on Gaussian type orbitals (GTOs), a tremendous effort has been done to reduce the size of the localized basis set, while keeping the same level of accuracy as one of the corresponding primitive bases. Indeed, the computational cost crucially depends on the basis set size L, growing as fast as L^4, if the four-index interaction integrals are fully evaluated. Very effective basis has been proposed, such as Dunning's,[2,3] Peterson's,[4] and Weigend's,[5] which allow one to systematically converge to the complete basis set (CBS) limit. Their construction required a thorough analysis of the correlation effects in free atoms, and their dependence on the orbital components, systematically added to the basis set.

Efficient schemes to generate optimal atomic basis in a more automatic way have been developed along the years. Those are usually based on the diagonalization of the density matrix computed for the atomic ground state, as first proposed by Almlöf and Taylor.[6,7] The resulting atomic natural orbitals (ANOs) are contractions of the Gaussian primitive basis set, provided automatically by the density matrix diagonalization. To improve their transferability and generate a more balanced basis set for molecular calculations, Widmark and coworkers[8–10] devised better schemes, based on the diagonalization of a density matrix appropriately averaged over several atomic states. An interesting recent development in the basis set generation shows that a high-quality basis can be generated by combining ANO orbitals obtained from the density matrix of an atomic multiconfigurational self-consistent field (MCSCF), with Gauss-Slater mixed primitive functions[11] optimized for the homonuclear dimers at the coupled cluster single double (CCSD) level of theory. The resulting compact ANO-GS basis set is particularly suited for quantum Monte Carlo (QMC) calculations.[12]

The idea of using the ANOs to improve the convergence of the basis set dates back to the seminal paper by Löwdin.[13]

a)sorella@sissa.it
b)mario.dagrada@impmc.upmc.fr
c)gmazzola@phys.ethz.ch
d)michele.casula@impmc.upmc.fr

Weinhold and coworkers developed the ANO formalism to find a set of natural hybrid orbitals (NHOs)[14] which are optimal not only for their convergence properties but also because they allow a clearer interpretation of the chemical bond[15] out of a quantum chemistry calculation in large basis sets, where the chemical picture is not usually transparent. Since then, several papers appeared, with the aim at finding the best scheme to generate a minimal basis bearing all physical information on the local atom embedded in a quantum system.[16–24]

In QMC calculations, compact and efficient basis sets are eagerly needed. In variational Monte Carlo (VMC), the task is to define a consistent many-body wave function, namely, a correlated ansatz providing the minimum possible energy expectation value of the non-relativistic Hamiltonian with long-range Coulomb forces and within the Born-Oppenheimer (BO) approximation. Generally speaking, a correlated ansatz is made of a determinantal part, usually the Slater determinant, which fulfills the antisymmetric properties of electrons, multiplied by a Jastrow factor which takes into account the dynamic correlation. While few basis functions, either GTO[25] or polynomials[26] are sufficient to define a good Jastrow factor, the determinantal part remains the most complicated object to develop, even if its atomic basis set expansion converges more rapidly when the Kato cusp conditions[27] are fulfilled exactly by the Jastrow part. Moreover, to have a good description of static correlations, wave functions beyond the Jastrow-Slater form have been proposed, where the Slater determinant is replaced by complete active space (CAS) wave functions,[28] antisymmetrized geminal power (AGP) wave functions,[25,29] and pfaffians.[30,31]

It is well known that a consistent QMC wave function, with both the Jastrow and the determinantal parts simultaneously optimized within a given basis set, provides much better properties. Thanks to recent methodological developments,[32–34] the energy minimization of the determinantal parameters can be systematically carried out. However, in order to allow the simultaneous energy optimization of the Jastrow and the determinantal parts, it is extremely important to reduce the atomic basis size M_A of the determinant, because, as we will see in the following, the number of variational parameters necessary to define a variational wave function scales as M_A^2.

In this paper, we introduce a method, based on a density matrix embedding of the determinantal part, which allows for a systematic reduction of the dimension of the atomic basis, by yielding atomic orbitals in an automatic and almost black-box procedure. This method is an application of the concept of quantum entanglement[35] between a part of a system (A) interacting with the environment (B), where one represents A (B) with a set of M_A (M_B) orthogonal states labeled by the index i (j) and writes down the wave function of the universe $U = A \cup B$ as

$$|U\rangle = \sum_{i=1,j=1}^{M_A,M_B} \psi_{ij} |i \otimes j\rangle. \tag{1}$$

It is straightforward to show[36] that the optimal way to describe the universe by using only few $p \ll M_A$ states of the system *embedded in the universe* is obtained by using the p eigenvectors corresponding to the largest eigenvalues of the density matrix,

$$D_{ii'} = \sum_j \psi^*_{ij} \psi_{i'j}. \tag{2}$$

The approach above is essentially equivalent to the Schmidt decomposition of the rectangular matrix ψ_{ij}. It is extremely simple and general, and it has been successfully applied in a variety of embedding schemes, going from the celebrated density matrix renormalization group (DMRG)[37] to the recent density matrix embedding theory (DMET),[38,39] and its simplified density embedding version.[40,41]

Our method is based upon a modification of the previously described concept of embedding, where the universe is restricted to the determinant of a geminal (or pairing) function, i.e., $|U\rangle = \det\{\phi(\mathbf{r}_i, \mathbf{r}_j)\}$. In this approach, the many-body coefficients ψ_{ij} of Eq. (1) are replaced by the f_{ij} coefficients, which define the pairing function,

$$\phi(\mathbf{r}, \mathbf{r}') = \sum_{i,j=1}^{M_A+M_B} f_{ij} \langle \mathbf{r}|i\rangle \langle \mathbf{r}'|j\rangle, \tag{3}$$

where the $M_A + M_B$ states $|i\rangle$ are now a one-body atom-centered basis set, which spans the whole space ($A \cup B$), and is not restricted to be orthonormal. Thus, in our approach, the universe is represented by an AGP function, which includes the Slater determinant as the lowest rank—i.e., $N/2$- limit of f_{ij}, when the $\phi(\mathbf{r}, \mathbf{r}')$ becomes equal to the standard one-body density matrix. As we show in the paper, this formalism allows one to define the embedding at the geminal level, by dealing with 2-body objects in a much simpler way than the direct N-body integration required to generate the one-body density matrix in the general correlated case. The resulting geminal embedded orbitals (GEOs) represent an orthonormal basis set and are defined as generalized hybrid orbitals, namely, contractions of non-orthogonal atomic orbitals, optimally chosen to minimize the basis set extension at a given target accuracy. We show that for single determinant wave functions, the method presented here is superior to the "standard" NHOs generation (which leads to the so-called "maximum-occupancy" orbitals[14]), thanks to the efficiency of the present embedding scheme.

In practice, the GEOs can be generated from previous "mean-field" calculations, such as Hartree-Fock (HF) and DFT, or from previous Jastrow correlated Slater determinant (JSD) or Jastrow AGP (JAGP) quantum Monte Carlo calculations carried out in an extended basis set. In the JSD and JAGP cases, the embedding is performed for the determinantal part only. This procedure yields GEOs which depend on the local environment and are therefore fundamentally different from the previously proposed ANOs basis sets, as the latter are determined for free, isolated atoms. If the GEOs are taken at the single Slater determinant level, our method is similar to the embedding proposed in Ref. 42, which is focused on fixing the best *linking* orbitals from a target region to a given environment. Here, the embedding is meant to give the best orbitals for the *target* region itself, where the target is usually every single atomic site, but it is not necessarily limited to it. Once determined at the DFT level, the GEO coefficients can be

further optimized in a subsequent QMC energy minimization, efficiently performed in an optimally contracted basis set and for a significantly reduced number of variational parameters.

The paper is organized as follows. In Sec. II, we describe the density matrix embedding and the way to find the optimal GEOs and Sec. III shows how the scheme works in practice through selected applications (the water molecule in Sec. III A, the α-to-γ transition in solid cerium in Sec. III B, and the liquid hydrogen at high pressure in Sec. III C). Finally Sec. IV is devoted to the concluding remarks.

II. GEMINAL EMBEDDED ORBITALS CONSTRUCTION

A. Wave function form

We use the paramagnetic Jastrow correlated Slater determinant as ansatz in our solid state calculations, with parameters determined to minimize the energy of the scalar-relativistic first-principles Hamiltonian. Unless otherwise specified, the full Coulomb electron-ion interaction is replaced by a scalar-relativistic Hartree-Fock energy-consistent pseudopotential of Burkatzki, Filippi, and Dolg (BFD) type.[43,44]

The JSD wave function reads

$$\Psi_{\rm JSD}(\mathbf{R}_{\rm el}) = \exp[-J(\mathbf{R}_{\rm el})]\,\det[\psi_i^{MO}(\mathbf{r}_j^{\uparrow})]\,\det[\psi_i^{MO}(\mathbf{r}_j^{\downarrow})], \qquad (4)$$

where $1 \le i,j \le N/2$, and $\mathbf{R}_{\rm el} = \{\mathbf{r}_1^{\uparrow},\ldots,\mathbf{r}_{N/2}^{\uparrow},\mathbf{r}_1^{\downarrow},\ldots,\mathbf{r}_{N/2}^{\downarrow}\}$ the many-body electron configuration, with N the total number of electrons. $\psi_i^{MO}(\mathbf{r})$ are orthonormal molecular orbitals (MOs) each one occupied by opposite spin electrons. The orbitals $\psi_i^{MO}(\mathbf{r})$ are expanded in a GTO basis set $\{\chi_j^{\rm det}\}$, centered on the atomic nuclei, i.e.,

$$\psi_i^{MO}(\mathbf{r}) = \sum_{j=1}^{M_A\times N_{\rm atoms}} \mu_{ij}\chi_j^{\rm det}(\mathbf{r}), \qquad (5)$$

where the sum in the above equation runs over both the local basis set (M_A) and nuclear center indices ($N_{\rm atoms}$). The $\{\chi_i^{\rm det}\}$ basis set is uncontracted (primitive) with a system dependent size M_A. The μ_{ij} and the exponents of the primitive Gaussian basis set $\{\chi_j^{\rm det}\}$ are variational parameters. The primitive atomic basis $\chi_i^{\rm det}(\mathbf{r})$ is not constrained by any orthogonalization condition, namely, the overlap matrix $s_{ij} = \langle\chi_i^{\rm det}|\chi_j^{\rm det}\rangle$ is an arbitrary strictly positive definite matrix. Nevertheless, the coefficients μ_{ij} can be determined in a way that the molecular orbitals remain orthonormal,

$$\langle\psi_i^{MO}|\psi_j^{MO}\rangle = \delta_{ij}, \qquad (6)$$

namely, $\mu s\mu^{\dagger} = I$. The first guess for ψ_i^{MO} is provided by DFT calculations in the local density approximation (LDA), performed in the same basis set.

To go beyond the JSD ansatz in Eq. (4), we use its JAGP extension in solid state calculations wherever the Fermi level in the supercell is degenerate, and in molecular applications. In the JAGP case, the wave function reads

$$\Psi_{\rm JAGP}(\mathbf{R}_{\rm el}) = \exp[-J(\mathbf{R}_{\rm el})]\,\det[\phi(\mathbf{r}_i^{\uparrow},\mathbf{r}_j^{\downarrow})]. \qquad (7)$$

The geminal function ϕ in Eq. (7) is written as

$$\phi(\mathbf{r},\mathbf{r}') = \sum_{i=1}^{M}\lambda_i^{\rm AGP}\psi_i^{MO}(\mathbf{r})\psi_i^{MO}(\mathbf{r}'). \qquad (8)$$

If $M = N/2$ and $\lambda_i^{\rm AGP} = 1$ for $i = 1,\ldots,N/2$, the expansion of Eq. (8) is equivalent to the single Slater determinant in Eq. (4), which factorizes into up and down components. However, to better describe static correlations in molecular calculations, M can be larger to include orbitals above the HOMO level. In the case of solid state calculations with degenerate shells at the Fermi level, M can be larger to comprise all degenerate orbitals, with all the HOMO $\lambda_i^{\rm AGP}$ taken equal and tiny. One can prove that the AGP part of $\Psi_{\rm JAGP}$ becomes then a linear combination of SDs, each containing one degenerate orbital.[29] In this way, the shell degeneracy is correctly taken into account, and the symmetry of the supercell is not broken.

This variational ansatz has proven very accurate in a large variety of *ab initio* systems, molecules,[25,45,46] and solids.[47–49] The Jastrow factor J is the one expanded over Gaussian basis set orbitals, first introduced in Ref. 25 and further developed later (see, e.g., Ref. 50 and references therein). It is not detailed here, as it is not the main focus of the present paper. Moreover, the embedding scheme of the determinantal part devised here is very general and can be used in combination with other types of Jastrow factors,[51–53] or directly on Slater determinants generated by HF or DFT. Both DFT and QMC calculations have been carried out using the TurboRVB package.[54]

B. Geminal embedding scheme

1. General framework

The starting molecular orbitals $\psi_i^{MO}(\mathbf{r})$ are optimized in a finite localized basis, where each element $\chi_i^{\rm det}(\mathbf{r})$ is centered at a given atomic position $\mathbf{R}_i$ (see Eq. (5)). The purpose of the present section is to determine a method that is able to minimize the number of atomic basis elements for a fixed target accuracy, once it is assumed that the original elements of the basis are given by localized orbitals.

Of course for large basis sets, the location $\mathbf{R}_i$ of the atomic orbitals becomes an ill-defined concept because in principle a complete basis can be generated in any position of the space and not necessarily around a given atom. In the following, we will consider a reasonable dimension for the original basis set $\{\chi_i^{\rm det}\}$ because (i) large localized basis has the well known problem to be highly redundant, preventing a stable energy minimization of the many body wavefunction within the Monte Carlo approach, which is the main application we will consider in the following; and (ii) within this scheme, it is usually enough to consider rather small and well-conditioned basis sets (i.e., the corresponding overlap matrix has a condition number much smaller than the inverse numerical relative precision) to have quite accurate physical results.

We note that $\{\chi_i^{\rm det}\}$ is not restricted to be a set of GTOs. Indeed, it can represent a more general atomic basis set, over which the GEOs will be expanded. However, all the results presented in this paper are obtained using GTOs as $\{\chi_i^{\rm det}\}$, as already stated in Sec. II A. In the following, we do not restrict

$\{\chi_i^{\rm det}\}$ to be orthonormal, either. We also take all functions described in this section real, for the sake of simplicity, as it is not difficult to generalize this derivation to the complex case.

We consider the general form of the geminal function in Eq. (8). As we have seen, it can describe also a single Slater determinant, with $\lambda_i^{\rm AGP} = 1$ for $i = 1, \ldots, N/2$, and $\{\lambda_i^{\rm AGP} = 0\}_{i>N/2}$. Like the Slater determinant, when the $\lambda_i^{\rm AGP}$ are all equal, the geminal is invariant for all unitary transformations O of the molecular orbitals,

$$\psi_i^{MO} \to \sum_j O_{i,j}\psi_j^{MO}. \tag{9}$$

Therefore, the geminal is a convenient representation of a Slater determinant, as it allows the use of a metric in the space of $\mathcal{R}^3 \times \mathcal{R}^3$ pairing functions, much simpler than the many-body distance defined in the $\mathcal{R}^{3N}$ Hilbert space, and nevertheless without destroying the invariance upon unitary rotations O. The same metric can be used in the more general form when the SD becomes a true AGP (i.e., with a geminal of rank $>N/2$).

The embedding we propose here is done at the geminal level, by left projecting Eq. (8) over a single atom centered at $\mathbf{R}$,

$$U_{\rm proj}^{\mathbf{R}}(\mathbf{r},\mathbf{r}') = \sum_i \lambda_i^{\rm AGP}\psi_{i,\mathbf{R}}^{\rm proj}(\mathbf{r})\psi_i^{MO}(\mathbf{r}'), \tag{10}$$

where $\psi_{i,\mathbf{R}}^{\rm proj}(\mathbf{r})$ are obtained by expanding the molecular orbitals $\psi_i^{MO}(\mathbf{r})$ on the atomic basis set $\{\chi_i^{\rm det}\}$ (Eq. (5)) and considering in $\psi_{i,\mathbf{R}}^{\rm proj}(\mathbf{r})$ only those components centered on the chosen atom, namely,

$$\psi_{i,\mathbf{R}}^{\rm proj}(\mathbf{r}) = \sum_{j|\mathbf{R}_j=\mathbf{R}} \mu_{ij}\chi_j^{\rm det}(\mathbf{r}). \tag{11}$$

Unless otherwise stated, hereafter, we are going to omit the symbol $\mathbf{R}$ in the projected quantities, for the sake of readability. The left-projected geminal defined in Eq. (10) plays the role of the entangled state corresponding to the system (selected atom) plus the environment (all atoms) in Eq. (1), where now the indices labeling the system A and the environment B are replaced by positions $\mathbf{r}$ and $\mathbf{r}'$, respectively.

We then determine the "best" geminal embedded atomic orbitals $\phi_i^{GEO}(\mathbf{r})$ by representing the left-projected geminal function $\sum_{i=1}^{p}\phi_i^{GEO}(\mathbf{r})\bar{\psi}_i(\mathbf{r}')$ in an optimally reduced space, namely, in terms of only $p \ll M_A$ atomic natural hybrid orbitals centered on the reference atom and of corresponding auxiliary molecular orbitals $\bar{\psi}_i(\mathbf{r}')$ spanning all the system. This can be achieved by a standard Schmidt decomposition, through a minimization of the Euclidean distance between the truncated and the projected geminal function. This minimization will be shown to be equivalent to diagonalize the density matrix kernel, defined, in analogy with Eq. (2), as

$$D_{\rm proj}(\mathbf{r},\bar{\mathbf{r}}) = \int d\mathbf{r}' U_{\rm proj}(\mathbf{r},\mathbf{r}')U_{\rm proj}(\bar{\mathbf{r}},\mathbf{r}'). \tag{12}$$

The corresponding eigenvalues w_i may be related to the GEOs occupation and their chemical reactivity.

2. Detailed procedure

In the following, we are going to explain our procedure to determine a substantial reduction of the basis dimension in more detail. We rewrite the term in Eq. (10) by expanding it in the chosen atomic basis,

$$U_{\rm proj}(\mathbf{r},\mathbf{r}') = \sum_k^M \lambda_k^{\rm AGP} \sum_{i|\mathbf{R}_i=\mathbf{R}} \sum_j \mu_{ki}\mu_{kj}\chi_i^{\rm det}(\mathbf{r})\chi_j^{\rm det}(\mathbf{r}'). \tag{13}$$

To shorthand the notation, Eq. (13) can be also written in terms of a matrix λ,

$$U_{\rm proj}(\mathbf{r},\mathbf{r}') = \sum_{ij} \lambda_{ij}\chi_i^{\rm det}(\mathbf{r})\chi_j^{\rm det}(\mathbf{r}'), \tag{14}$$

where $\lambda_{ij} = [\mu^\dagger\lambda^{\rm AGP}\mu]_{ij}$[55] if the orbital $\chi_i^{\rm det}(\mathbf{r})$ is such that $\mathbf{R}_i = \mathbf{R}$, while $\lambda_{ij} = 0$ if $\mathbf{R}_i \neq \mathbf{R}$, whereas the column index j runs all over the atomic basis.

The term defined in Eq. (13) carries information on the intra-atomic electronic structure affected by inter-atomic interactions between the site $\mathbf{R}$ and its environment. The inter-atomic interactions are explicitly kept by the left-partial projection of the full density matrix. We found this embedding scheme particularly effective to determine the best GEOs spanning an optimally truncated Hilbert space.

We employ the Schmidt decomposition of Eq. (13) in a truncated space spanned by p terms only, as

$$\bar{U}_{\rm proj}(\mathbf{r},\mathbf{r}') = \sum_{k=1}^{p} \phi_k^{GEO}(\mathbf{r})\bar{\psi}_k(\mathbf{r}'). \tag{15}$$

In order to find the best GEOs, we minimize the Euclidean distance $d = |U_{\rm proj} - \bar{U}_{\rm proj}|$ between the original and the truncated geminal functions. These functions are defined in $\mathcal{R}^3 \times \mathcal{R}^3$ in such a way that

$$d^2 = |U_{\rm proj}|^2 - 2\sum_k \int d\mathbf{r}d\mathbf{r}' U_{\rm proj}(\mathbf{r},\mathbf{r}')\phi_k^{GEO}(\mathbf{r})\bar{\psi}_k(\mathbf{r}') + \sum_k \int d\mathbf{r}\,\bar{\psi}_k^2(\mathbf{r}), \tag{16}$$

where $|U_{\rm proj}|^2 = \int d\mathbf{r}d\mathbf{r}' U_{\rm proj}^2(\mathbf{r},\mathbf{r}')$, and we assumed that the optimal atomic orbitals are orthonormal. This assumption is without loss of generality, because—whatever is the solution for the minimum—we can always orthogonalize the corresponding optimal orbitals ϕ_i^{GEO} and get a solution written in the same form as in Eq. (15). We can then take the variation over all possible unconstrained functions $\bar{\psi}(\mathbf{r})$ and show that the steady condition $\frac{\delta d^2}{\delta\bar{\psi}_k(\mathbf{r})} = 0$ implies

$$\bar{\psi}_k(\mathbf{r}) = \int d\mathbf{r}' U_{\rm proj}(\mathbf{r}',\mathbf{r})\phi_k^{GEO}(\mathbf{r}'). \tag{17}$$

Replacing Eq. (17) into (16) yields

$$d^2 = |U_{\rm proj}|^2 - \sum_k \int d\mathbf{r}d\mathbf{r}' D_{\rm proj}(\mathbf{r},\mathbf{r}')\phi_k^{GEO}(\mathbf{r})\phi_k^{GEO}(\mathbf{r}'), \tag{18}$$

where $D_{\rm proj}$ is the density matrix we have defined in Eq. (12). Thus, in order to minimize d^2, one needs to maximize the quadratic form involving $D_{\rm proj}$, with the constraint that the orbitals $\phi_k^{GEO}(\mathbf{r})$ are orthonormal. Therefore, by the

minimum/maximum property of symmetric operators (such as the positive definite density matrix), it is clear that d^2 is minimized just when the optimal GEO orbitals coincide with the p eigenvectors of the density matrix with maximum eigenvalues w_i. Indeed, all the eigenvalues w_i must be positive, and the corresponding eigenvectors are obviously an orthonormal set of states, consistently with the assumption.

From Eq. (12) and the choice of the atomic projectors, it follows that the density matrix kernel $D_{\rm proj}$ can be expressed in terms of the atomic basis $\{\chi_i^{\rm det}\}$ restricted around a given atom at the selected position $\mathbf{R}_i = \mathbf{R}$. By consequence, also the optimal GEOs can be expanded on the same local basis,

$$\phi_i^{GEO}(\mathbf{r}) = \sum_{j|\mathbf{R}_j=\mathbf{R}} \mu_{ij}^{GEO} \chi_j^{\rm det}(\mathbf{r}). \tag{19}$$

In the non-orthogonal finite basis $\{\chi_j^{\rm det}\}$, this turns into the generalized eigenvalue equation,

$$\sum_{j|\mathbf{R}_j=\mathbf{R}} \left[(\lambda s \lambda^\dagger) s\right]_{ij} \mu_{kj}^{GEO} = w_k \mu_{ki}^{GEO}$$
$$\text{for } i \text{ such that } \mathbf{R}_i = \mathbf{R}, \tag{20}$$

where the matrix λ has been defined through Eq. (14). Eq. (20) can be immediately solved by standard linear algebra packages,[56] by considering that the overlap matrix s is symmetric and positive definite. After diagonalization, the eigenvector coefficients satisfy the orthogonality requirement $\mu^{GEO} s (\mu^{GEO})^\dagger = I$ that we have previously assumed. Moreover, the truncation error, i.e., the residual distance, is $d^2 = |U_{\rm proj}|^2 - \sum_{i=1}^{p} w_i$.

3. GEO properties

Because the $\{\phi_i^{GEO}\}$ basis set is optimal in the sense defined in Secs. II B 1 and II B 2, it has the advantage of not only being the best compromise between size and accuracy but also carrying the physical information on the most representative atomic states for a site embedded and interacting with its environment.

Indeed, we notice that according to Eq. (19), the best GEOs are hybrid orbitals, as they are expanded over the full set of atomic angular momenta. Thus, they can take care of nontrivial chemical hybridizations and, for instance, the crystal field effect in solids is also automatically taken into account, as we will see in Sec. III B.

In the case of a starting geminal representing a Slater determinant, after the determination of the optimal basis $\{\phi_i^{GEO}\}$, one can rewrite the same Slater determinant in Eq. (4), within a target accuracy, by expressing all the molecular orbitals in terms of the GEO basis and with a dramatic reduction of the basis dimension and the number of variational parameters.

As introduced in Sec. II B 1, our embedding scheme naturally deals with a determinantal part not necessarily restricted to a SD form. Indeed, as the best GEOs are obtained by a distance minimization in the $\mathcal{R}^3 \times \mathcal{R}^3$ space, this can be applied not only to geminals of Slater type but also to more generalized types with an arbitrary number of MOs ($M \geq N/2$), and with free parameters $\{\lambda_i^{\rm AGP}\}$. This would correspond to the AGP form in Eq. (8), as explained in Sec. II A. While for Slater determinants, a relation can be found with the NHOs (see Sec. II B 5), the more general AGP is less trivial, but it is rigorously accounted for by the formalism presented in this work, which is generally applicable to *any* form of geminal functions. Therefore, via this scheme, one can find a GEO basis set which is optimal for both SD and AGP types of wave functions.

4. Choice of the atomic projectors

In the geminal embedding method, we use Eq. (11) to single out the local states at $\mathbf{R}$ in the left-projected geminal of Eq. (10). The one in Eq. (11) is not the only possible way to define a projection around an atomic center $\mathbf{R}$. For instance, one could have used the "standard" atomic projectors

$$\mathcal{P}_{\mathbf{R}}^{\rm at} = \sum_{i|\mathbf{R}_i=\mathbf{R}} \sum_{j|\mathbf{R}_j=\mathbf{R}} |\chi_i^{\rm det}\rangle s_{i,j}^{-1} \langle \chi_j^{\rm det}|, \tag{21}$$

with s the overlap matrix, and defined $\psi_{i,\mathbf{R}}^{\rm proj} = \mathcal{P}_{\mathbf{R}}^{\rm at} \psi_i^{MO}$. However, we found that the optimal choice is the one of taking only the basis set elements centered on the atom $\mathbf{R}$ in Eq. (5), therefore, defining $\psi_{i,\mathbf{R}}^{\rm proj} = \sum_{j|\mathbf{R}_j=\mathbf{R}} \mu_{ij} \chi_j^{\rm det}$, as in Eq. (11).

In order to understand this property, just consider the case when the basis is redundant around the given atomic center $\mathbf{R}$ (complete in $\mathbf{R}$, overcomplete when all atomic centers are taken into account). This implies that Eq. (10) can be expanded in a much smaller number of elements, and this refinement of the basis around $\mathbf{R}$ can be easily determined by focusing on $U_{\rm proj}^{\mathbf{R}}(\mathbf{r},\mathbf{r}')$, as it has been described in Sec. II B 1. Instead, if we use the projector $\mathcal{P}_{\mathbf{R}}^{\rm at}$, this becomes the identity in the limit of large basis and it is therefore not possible to disentangle a better localized basis set.

In the example mentioned above, namely, in the case of a redundant basis and by using the projector in Eq. (11), we can still describe Eq. (10) in terms of only $p < M_A$ appropriate atomic orbitals, given by the eigenvectors of $D_{\rm proj}$ corresponding to its p non-zero eigenvalues. On the other hand, if we use this criterion of basis reduction for all the atomic positions $\mathbf{R}_i$, we obtain the full geminal $\phi(\mathbf{r},\mathbf{r}') = \sum_{\mathbf{R}} U_{\mathbf{R}}^{\rm proj}(\mathbf{r},\mathbf{r}')$ *exactly*. In the practical implementation (Sec. II B 2), we remove also eigenvectors of $D_{\rm proj}$ with small eigenvalues, by making therefore an approximation. It is clear however that this approximation can be systematically controlled by decreasing the threshold of the accepted eigenvalues of $D_{\rm proj}$.

5. Relation with standard natural hybrid orbitals

The "standard" atomic NHOs are defined as eigenstates of the *local atomic density matrix* $D^{\rm atomic}$, both left and right projected on a given site.

The density matrix $D(\mathbf{r},\mathbf{r}')$ in general notations is a two-point correlation function that, for wave functions in the SD representation, coincides with the geminal $\phi(\mathbf{r},\mathbf{r}')$, by setting $M = N/2$ and $\lambda_i^{\rm AGP} = 1$ for $i = 1,\ldots,M$ in Eq. (8). Equivalently, the density matrix coincides with our unrestricted expression of U in Eq. (10), namely, obtained

with $\psi_i^{\rm proj} = \psi_i^{MO}$. In the same SD limit, $D = U = U^2$, for orthonormal MOs.

Therefore, in order to determine the NHOs, one needs to define the local atomic density matrix as $D_{\mathbf{R}}^{\rm atomic} = \mathcal{P}_{\mathbf{R}}^{\rm at} D \mathcal{P}_{\mathbf{R}}^{\rm at}$. In the SD limit, this is equivalent to

$$D_{ij}^{\rm atomic} = \langle \chi_i^{\rm det} | \phi | \chi_j^{\rm det} \rangle \quad \text{for } i \text{ such that } \mathbf{R}_i = \mathbf{R}, \text{and } j \text{ such that } \mathbf{R}_j = \mathbf{R}. \quad (22)$$

This is clearly different from our definition of projected density matrix $D_{\rm proj}$ in Eq. (12), as in the latter case we do not use the standard atomic projection operators.

The second important difference takes place for wave functions beyond the SD representation, when the geminal ϕ is no longer equivalent to the density matrix D. Therefore, also $D_{\rm proj}$, based on atomic projected ϕ, will differ from $D^{\rm atomic}$, based on atomic projected D, no matter what the atomic projector is.

We will compare the GEOs generated by the scheme in Sec. II B 2 with the NHOs obtained as solution of the following linear system:

$$\sum_{j|\mathbf{R}_j=\mathbf{R}} D_{ij}^{\rm atomic} \mu_{kj}^{\rm NHO} = w_k s_{ij} \mu_{kj}^{\rm NHO} \quad \text{for } i \text{ such that } \mathbf{R}_i = \mathbf{R}, \quad (23)$$

by taking the first p NHOs with the largest w_k,

$$\phi_k^{NHO}(\mathbf{r}) = \sum_{j|\mathbf{R}_j=\mathbf{R}} \mu_{kj}^{\rm NHO} \chi_j^{\rm det}(\mathbf{r}). \quad (24)$$

This choice corresponds to the "maximum-occupancy" orbitals.[14] In Sec. III A and for SD wave functions, when a direct comparison between GEOs and NHOs is possible, we will show that our embedding scheme yields GEOs that provide much better performances in reducing the size of the atomic basis, compared to the standard NHOs discussed above.

III. SELECTED APPLICATIONS

In this section, we illustrate the relevance of our embedding scheme by showing three examples: the determination of the best GEO basis set in water (Sec. III A), cerium (Sec. III B), and hydrogen (Sec. III C). In the first case, the natural orbitals determined by the density matrix embedding method significantly reduce the number of wave function parameters and so its computational burden. In the second case, the GEO basis set carries the physical information on the atomic structure of a cerium site embedded in the crystal environment and allows a physical interpretation of the electronic change underlying the α-to-γ volume collapse. In the last example, the GEO basis is shown to be the best compromise between accuracy and efficiency in the determination of the phase diagram of liquid hydrogen at high pressure by means of QMC-based molecular dynamics (MD) calculations, which require both accurate and cheap wave functions.

A. Water molecule

A proper description of the water molecule is essential to reproduce the structural and electronic properties of larger water cluster, liquid water, and ice, because in large systems containing several molecules, there is a strong interplay between the intramolecular and intermolecular degrees of freedom, due to the large water dipole moment and the strong directionality of the H bond. For this reason, the water molecule has been the subject of many theoretical works,[57–61] aiming at finding the quantum chemistry method which has the best balance between accuracy and computational cost.

In this regard, QMC methods are promising, thanks to their favorable scaling with the system size. Here, we report our pseudopotential and all-electron calculations[62] on the water molecule with different wave function types and basis sets, in order to show that the speed-up offered by the GEOs basis set is relevant and can open the way to more systematic studies on larger water systems.

The BFD pseudopotential[64] has been used for oxygen, while the two hydrogens have been treated as all-electron. We have also performed full all-electron calculations, for both oxygen and hydrogen. The primitive Gaussian basis set for oxygen is $(5s,5p,2d)$ and $(6s,6p,2d)$ in pseudopotential and all-electron calculations, respectively. For hydrogen, the primitive basis set is $(4s,2p)$. The Jastrow functional form has been kept fixed and developed on a primitive Gaussian basis set of $(3s,2p,1d)$ and $(2s,1p)$ for oxygen and hydrogen, respectively. Note that this GTO set has been recently claimed to be one of the most accurate in an extensive QMC study of single molecule water properties,[65] which used the same Jastrow ansatz as ours. For the antisymmetric part, we tested two main wave function forms, the single Slater determinant (obtained by using a geminal with rank $N/2$) and the AGP function. At variance with Eq. (8), for the water molecule, we chose to develop the AGP geminal directly on the primitive GTOs (and not on MOs) to have a greater flexibility, such that

$$\phi(\mathbf{r},\mathbf{r}') = \sum_{a,b=1}^{M_A \times N_{\rm atoms}} \lambda^{a,b} \chi_a^{\rm det}(\mathbf{r}) \chi_b^{\rm det}(\mathbf{r}'). \quad (25)$$

The energy difference between the JSD and the JAGP wave functions, reported in Table I, shows the size of static correlations in the system, which amounts to 5-6 mH. Moreover, the AGP ansatz provides a better description of the nodal surface, because lattice regularized diffusion Monte Carlo (LRDMC) calculations[66,67] give a fixed-node energy which is 2.5 mHa lower than the one obtained by using the JSD trial wave function.[62] The JAGP wave function leads also to better geometrical properties.[62] Its relaxed geometry is closer to the experiment than the JSD one, in both the OH distance and the HOH angle.

To analyze how the AGP correlations develop in the water molecule, we diagonalize the geminal of Eq. (25) in order to recast it in its MOs representation of Eq. (8). Indeed, the diagonalization of ϕ in the space spanned by the basis set $\chi_a^{\rm det}$ yields the MOs as eigenvectors and $\lambda_i^{\rm AGP}$ as eigenvalues, whose absolute values are plotted in Fig. 1.

Fig. 1 shows that indeed the orbitals above the HOMO have a sizable weight, with a distribution which falls abruptly to zero only after the 40th orbital (not reported in the figure). This reflects the multideterminant character of the water molecule, taken into account by the AGP ansatz.

TABLE I. VMC energies of the water molecule and number of variational parameters in the QMC wave functions. The geometry is the experimental one in the pseudopotential calculations, while is the QMC relaxed one in all-electron calculations. See Ref. 62 for more details. The total number of parameters (last column) and the wave function quality varies depending on the contraction level of the GEOs used in the determinantal part. The Jastrow functional form has been kept fixed in all set of calculations. This gives a number of 195 and 418 Jastrow parameters for the pseudopotential and all-electron calculations, respectively. The other parameters are in the determinant, coming from both $\lambda^{a,b}$ (third to last column) and the basis set, i.e., $\chi_a^{\rm det}$ for the primitive GTO and ϕ_a^{GEO} for the GEOs (second to last column).

	VMC energies			Number of parameters		
Wave function ansatz	Energy E_x (Ha)	Variance (Ha^2)	$E_x - E_{\rm JSD}$ (mHa)	$\lambda^{a,b}$	$\chi_a^{\rm det}, \phi_a^{GEO}$	Total
Pseudopotential calculations						
JSD: primitive GTOs	−17.248 21(7)	0.2655(6)	0.0	682	18	895[a]
JAGP: (4O,1H) GEOs	−17.250 13(8)	0.2635(12)	−1.91(11)	21	158	374
JAGP: (4O,5H) GEOs	−17.251 83(6)	0.2510(6)	−3.62(10)	105	238	538
JAGP: (8O,2H) GEOs	−17.252 67(7)	0.2426(18)	−4.46(10)	78	298	571
JAGP: (8O,5H) GEOs	−17.253 02(6)	0.2412(34)	−4.89(10)	171	358	724
JAGP: primitive GTOs	−17.253 89(6)	0.2296(5)	−5.68(10)	682	18	895
All-electron calculations						
JSD: primitive GTOs	−76.400 25(8)	1.412(3)	0.0	1383	19	1820[a]
JAGP: (9O,2H) GEOs	−76.405 04(9)	1.399(6)	−4.79(12)	91	361	870
JAGP: primitive GTOs	−76.406 60(7)	1.374(3)	−6.35(11)	1383	19	1820

[a]Here, the number of parameters is the same as the one in the JAGP wave function since in the JSD ansatz, we rewrite the corresponding geminal (of rank $N/2$) on the uncontracted basis in order to optimize the MO's, as explained by Marchi *et al.*[63]

We turn now the attention on how to reduce the AGP basis set in an effective way. So far, both the JSD and JAGP wave functions have been developed on the primitive basis in order to exploit at most its flexibility. Thus, the total number of variational parameters is 895 in pseudopotential calculations (see the last column of Table I), quite large for a single molecule, particularly if one would like to tackle the study of larger water clusters by means of QMC techniques. The most important limitation of this approach is that the number of variational parameters corresponding to the matrix elements $\lambda^{a,b}$ increases as the square of the atomic basis size. Therefore, this should be reduced at minimum in order to make this approach feasible for a large number of molecules.

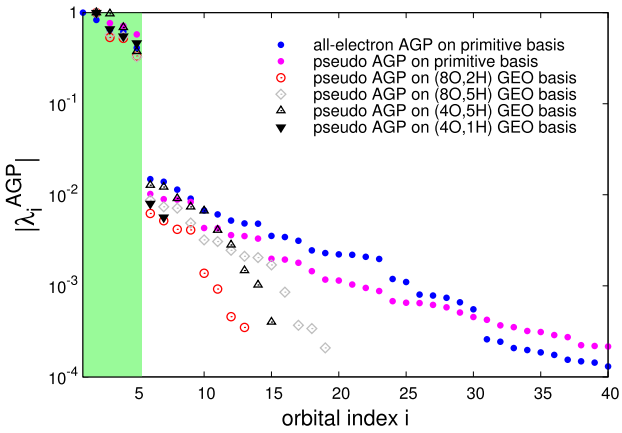

FIG. 1. Semilog plot of the modulus of the AGP eigenvalues versus the MO index for different basis sets and calculations. The orbital indexes include always the oxygen 1s electrons, replaced in the pseudopotential calculations. The green area represents the exactly occupied molecular orbitals in the single Slater determinant representation, with $\lambda_i = 1$ for $i \in \{1, \ldots, \text{HOMO}\}$ and $\lambda_i = 0$ for $i \geq \text{LUMO}$. In the AGP, also the orbitals above the HOMO are occupied, with a weight $|\lambda_i^{\rm AGP}|$ which jumps at the HOMO-LUMO level. The AGP developed on the GEO basis set correctly reproduces the HOMO-LUMO jump and spans the same relevant region in the AGP eigenvalues spectrum. Adapted from Ref. 62.

To this purpose, we would like to find the optimal contracted basis set. We start from our best JAGP wave function previously optimized, we take its Jastrow factor off, and we are left with its geminal part of Eq. (25). From there, we follow the recipe explained in Sec. II, and we generate a new set of GEOs, upon which we develop a new geminal,

$$\tilde{\phi}(\mathbf{r}, \mathbf{r}') = \sum_{a,b=1}^{p \times N_{\rm atom}} \tilde{\lambda}^{a,b} \phi_a^{GEO}(\mathbf{r}) \phi_b^{GEO}(\mathbf{r}'), \qquad (26)$$

where the $\tilde{\lambda}^{a,b}$ are given by overlap maximization of the latter $\tilde{\phi}$ with the original ϕ in the $\mathcal{R}^3 \times \mathcal{R}^3$ space. Thanks to the GEO expansion, the overlap is supposed to be good even for small GEO basis set size p. We found that, at fixed p, the normalized overlap $\langle\tilde{\phi}|\phi\rangle^2/(\langle\phi|\phi\rangle\langle\tilde{\phi}|\tilde{\phi}\rangle)$ is systematically larger when one uses the GEOs obtained as in Sec. II B than the NHOs obtained by diagonalization of the atomic (left *and* right projected) $U^{\rm atomic}$ matrix (the "maximum-occupancy" NHOs[14] of Eq. (24)). The overlap between the geminal function ϕ developed in the primitive basis and the one ($\tilde{\phi}$) written in the GEOs basis sets is reported in Table II. For the case in the latter table, the starting ϕ is the optimal one for the JSD energy of the water molecule in the primitive basis. Our embedding scheme systematically gives GEOs which yield a better overlap between ϕ and $\tilde{\phi}$, at a fixed GEO size, if compared with the overlaps obtained with the "standard" NHO embedding scheme.

From Eq. (26), it is apparent that the reduction of variational parameters with respect to the expression in Eq. (25) is a factor p^2/M_A^2, which can be extremely relevant if $p \ll M_A$. In the following, we are going to study the VMC energy convergence of the JAGP wave function expanded in GEOs as a function of p, by comparing it with its

TABLE II. Overlap $\langle\tilde{\phi}|\phi\rangle^2/(\langle\phi|\phi\rangle\langle\tilde{\phi}|\tilde{\phi}\rangle)$ between the geminal ϕ of the fully optimized JSD wave function in the primitive basis set and the best $\tilde{\phi}$ developed on the GEO/NHO basis set reported in the first column (with $\tilde{\lambda}^{a,b}$ which maximize the $\mathcal{R}^3\times\mathcal{R}^3$ overlap). Given the basis set size, the contracted atomic orbitals are determined in the "standard" way (third column, see Eqs. (23) and (24) for definition) and by the geminal embedding scheme described in Sec. II B 2 (second column). The embedding scheme presented here systematically gives better overlaps. The GEOs converge to full overlap already for a (4O, 4H) basis set, as the dimension of the "universe" is 4 in a SD wave function (the total number of electrons is 8 plus the $1s^2$ core electrons of oxygen), and in the GEO embedding framework, the maximum number of local states per nucleus is at most the dimension of the "universe". The last line corresponds to the complete basis set limit for the contractions with respect to the space spanned by the primitive basis set, where all methods have to converge by definition (as it is actually found numerically).

GEO/NHO basis set	GEOs overlap (%)	"Standard" NHOs overlap (%)
(4O,1H)	99.8390	99.0696
(8O, 2H)	99.9511	99.1846
(4O, 4H)	100.0000	99.1929
(4O, 5H)	100.0000	99.1933
(8O, 5H)	100.0000	99.2188
(12O, 6H)	100.0000	99.8305
(20O, 8H)	100.0000	99.9458
(30O, 10H)	100.0000	100.0000

rigorous lowest energy limit provided by the uncontracted JAGP reference previously computed. We recall that once the GEOs expanded AGP is obtained, its parameters are further optimized in the presence of the Jastrow factor by QMC energy minimization, in order to find the best variational wave function within the JAGP ansatz in the GEO basis set.

The energy results are reported in Table I. For the pseudopotential calculations, the (4O,1H) GEO basis set ($p = 4$ for oxygen, $p = 1$ for hydrogen) is the smallest basis set which can take into account the $2s2p$ near degeneracy at the atomic O level, including the 1s for H and the $2s$ and $2p$ orbitals for O. Its energy and variance are the poorest among the GEO basis sets considered in the table, though being lower than the JSD ansatz. On the other hand, the largest GEO basis used here, namely, the (8O,5H) set, recovers a large fraction of static correlation and its energy is less than 1 mHa above the uncontracted JAGP one. However, the parameter reduction is weak (see last column of Table I), with a total of 18 GEO basis set elements against 50 elements (counting also the azimuthal multiplicity) in the corresponding primitive basis set. The best compromise between efficiency, i.e., total number of variational parameters, and accuracy, i.e., variational energy, is provided by the (8O,2H) basis, as it yields a significant gain in energy with a small/moderate number of parameters.

The same behavior has been confirmed in all-electron calculations, reported in the lower panel of Table I, where the 1s electrons are explicitly kept in the oxygen atom. The corresponding GEO basis set has been extended to 9O GEO orbitals, performing in the same way as in the case of pseudopotential calculations in the 8O GEO basis set. Even in this case, the gain in the number of variational parameters is important, without a significant deterioration of the wave function with respect to the JAGP in primitive basis.

Finally, we study how the AGP spectrum changes with the contracted GEO basis sets. Fig. 1 shows that after a complete wave function optimization, the natural orbital eigenvalues magnitude of the GEO AGP covers the 10^{-2}–10^{-4} range of the primitive AGP, except for the shortest (4O,1H) basis, which clearly spans a too small Hilbert space. Moreover, we checked that the JAGP expanded on the optimal (8O,2H) basis gives the same fixed node LRDMC energy as the full JAGP, signaling that the nodal surface is properly described even by the (8O,2H) GEO contraction.

The advantage of using the GEO basis set will be remarkable for larger systems with many water molecules, as the number of variational parameters corresponding to the GEO orbitals grows only *linearly* with the number of atoms. Instead, the number of parameters corresponding to $\tilde{\lambda}^{a,b}$, grows quadratically, but it remains still affordable since it is dramatically reduced by this approach.

B. Solid cerium

The α-to-γ phase transition in cerium, also known as volume collapse, is one of the most challenging phase transitions in nature, as it is driven by the f-electron correlation,

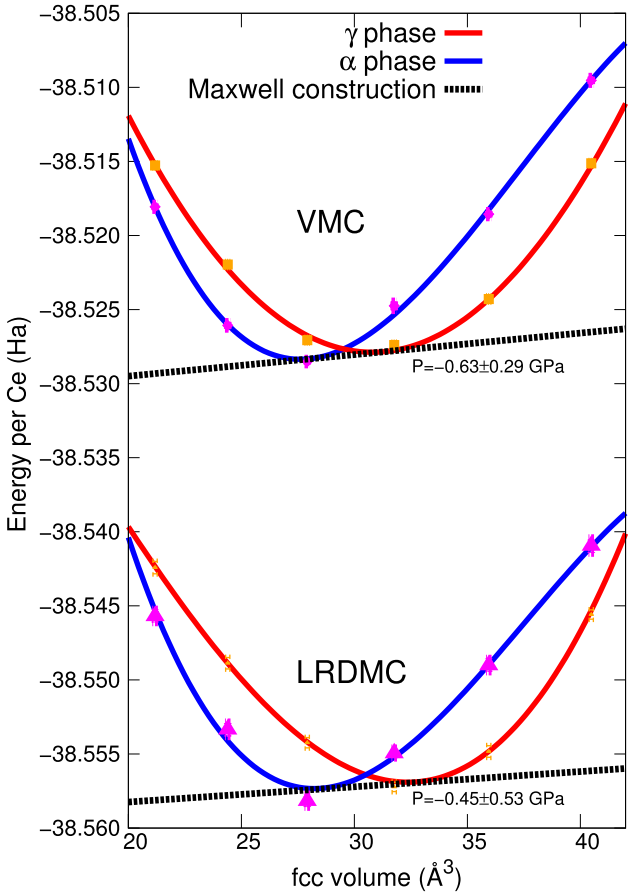

FIG. 2. Equation of state of the α (blue line) and γ (red line) phases of elemental cerium computed by VMC and LRDMC. In the y-axis, we report energies per atom of the pseudo-Hamiltonian. Also the common tangent construction is plotted (dashed black line), where the transition pressure is derived from. The experimental transition pressure extrapolated to 0 T is $\approx$−1 GPa.

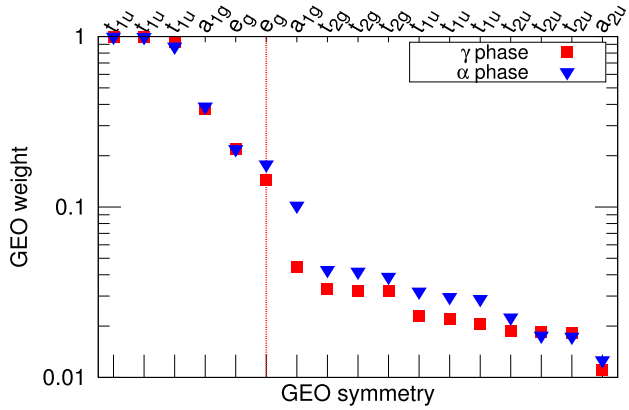

FIG. 3. Weights w_i of the first 17 most relevant GEOs, computed by following the embedding scheme detailed in Sec. II B. They are derived from the Slater determinants of the two wave functions describing the α (blue triangles) and γ (red squares) phases, respectively, at the unit cell volume of 31.7 Å^3 (fcc lattice space of 9.5 a_0). The vertical red line indicates the "closed-shell" occupation of the 12 electrons in the pseudopotential in the case of largely separated weakly interacting atoms. Adapted from Ref. 77.

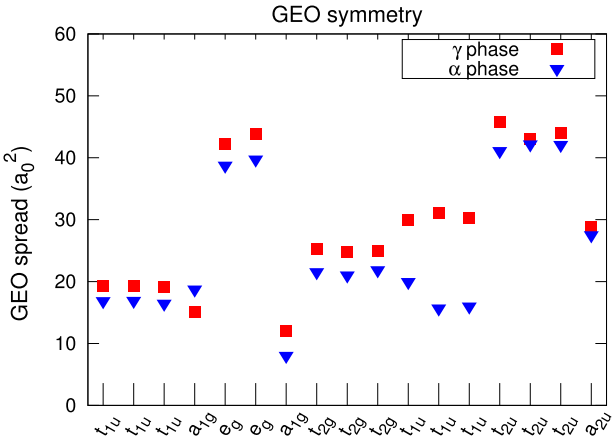

FIG. 4. Spread ($\langle\phi|r^2|\phi\rangle - |\langle\phi|\mathbf{r}|\phi\rangle|^2$) of the same GEO basis as in Fig. 3, for both the α (blue triangles) and γ (red squares) phase. Adapted from Ref. 77.

very hard to treat by any many-body method. Cerium peculiar features, such as its isostructural volume jump between two *fcc* structures, are not completely explained yet, and there is a strong debate whether the α-to-γ transition would still be present at zero temperature[68–72] and negative pressures (in the actual material, the transition occurs only at finite T[73]), or there is a lower critical point of the first-order transition line with $T_{\min} > 0$.[74] The question is not just academic, as the presence of a $T = 0$ first-order transition implies a purely electronic mechanism underlying the volume collapse, while temperature effects are certainly due also to electronic entropy contributions which are known to be important in f-electron systems.[75,76] Very recently,[77] accurate QMC calculations show that a first-order transition still exists even at 0 K. This is reported in Fig. 2, where the equation of state $E = E(V)$ is plotted for both VMC and LRDMC calculations.

As explained in Ref. 77, the two solutions found at fixed unit cell volumes, in a range compatible with the α and γ phases, mainly differ for their Slater determinants, which are fully optimized at the VMC level in the presence of the Jastrow factor by energy minimization. Their MOs are developed on a large $7s7p4d5f1g$ GTO primitive basis set, as in Eq. (5). From Fig. 2, it is apparent that the LRDMC further lowers the variational energy of the state, although without changing the physical picture of the transition. Indeed, the transition pressure and the critical volumes are in agreement with the experimental ones already at the VMC level. Interestingly enough, the nodal structure of the two phases, set by the Slater determinant, is certainly different, as the fixed node approximation is the only constraint in the LRDMC calculations which prevents one phase to be projected to the other.

In order to understand what is the electronic mechanism of the volume collapse, an analysis of the Slater part of the JSD wave function is thus necessary, as it bears information related to the electronic structure change between the two phases. With this aim, the embedding scheme proposed in the present paper is extremely useful, as the derived GEOs, their weights (Fig. 3) and their spread (Fig. 4) reveal the effect of the crystal field and the hybridization on the underlying electronic structure. The GEO in this case is naturally hybrid, as the crystal field mixes the atomic components. Thanks to the atomic orbital resolution of each GEO, it has been possible to assign to each one its correct spatial symmetry, compatible with the fcc crystal point group, which is reported in Figs. 3 and 4.

A feature which is clear from Fig. 3 is the tight competition between many different atomic states, the s-based a_{1g}, the d-based e_g and t_{2g}, and the f-based t_{1u}, t_{2u}, and a_{2u} orbitals. From band structure calculations, it is known that they all have weight at the Fermi level, and they are very close in energy. From our embedding analysis, they all contribute

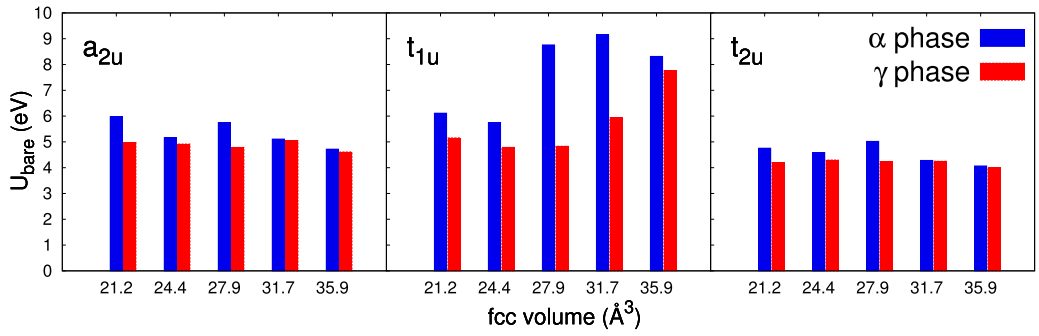

FIG. 5. Local Coulomb repulsion $U^k_{\text{bare}} = \langle\phi^{\text{GEO}}_k\phi^{\text{GEO}}_k|\frac{1}{|\mathbf{r}-\mathbf{r}'|}|\phi^{\text{GEO}}_k\phi^{\text{GEO}}_k\rangle$ computed on the GEO basis set of a_{2u}, t_{1u}, and t_{2u} symmetries, containing the f-orbital components, for the α and γ phases at different volumes (corresponding to the points in Fig. 2).

to the total wave function with quite similar weights w_i. This makes cerium a puzzling system, as its physics is dictated not only by the strong correlation affecting the f-orbitals but also by their complex interplay with more delocalized s, p, and d states. Only the first 4 GEO orbitals (3 t_{1u} and 1 a_{1g}) have weight close to 1, as they are almost perfectly occupied by the $5s^2 5p^6$ semi-core electrons included in the HF energy consistent pseudopotential,[44] which are chemically inert. The other 4 electrons in the pseudopotential go into the valence and occupy the higher energy GEOs according to an atomic participation rate which is related to the GEOs w_i. Fig. 3 shows that a main change between the α and γ phase is related to the weight of the a_{1g} (mainly $6s$) orbital, which reflects a different atomic occupation and thus a different nature of the chemical bond between neighboring atoms.

Another difference is apparent from Fig. 4, where we plot the GEOs spread. The most significant spread variation affects the t_{1u} orbitals, which are built upon a linear combination of p and f atomic symmetries, allowed by the crystal field. The t_{1u}, t_{2u}, and a_{2u} GEO orbitals are the most correlated, as they are made of f atomic orbitals. A change in the t_{1u} spread is a strong indication that the correlation level in the two phases is very different.

This is substantiated by the calculation of the local Hubbard repulsion $U^k_{\text{bare}} = \langle \phi^{\text{GEO}}_k \phi^{\text{GEO}}_k | \frac{1}{|\mathbf{r}-\mathbf{r}'|} | \phi^{\text{GEO}}_k \phi^{\text{GEO}}_k \rangle$, computed by using the GEO orbitals as local atomic states, and plotted in Fig. 5. In accordance to the spreads in Fig. 4, the main change in U affects the t_{1u} atomic states, with the α phase which has a larger U (at the *fixed* volume) than the γ phase. This is rather counter-intuitive, as the α phase is known to be less "correlated" than the γ one, as revealed, for instance, by a taller quasiparticle peak in photoemission spectroscopy at the Fermi level. However, these experimental signatures are obtained at different volumes, with the α phase in its collapsed configuration (15% volume less than the γ) and so with a U-over-bandwidth ratio which is larger in the γ phase. In our analysis, the two phases can be studied at the same volume, where two steady solutions are found. This possibility allows one to unveil an important effect due to the strong f-correlation: the γ phase gains energy with respect to the α phase, by reducing the local Coulomb repulsion in the t_{1u} channel, in the large-volume region where the correlation is stronger for both phases. This is thanks to the breathing of the t_{1u} orbitals, strongly hybridized with the p states, and broader in the γ phase. At its turn, this implies a larger $t_{1u} - t_{1u}$ overlap between neighboring sites, and so a stronger bonding character of the t_{1u} orbitals in the γ phase, whereas in the α phase, it is the a_{1g} (s) channel which has a stronger weight, as we have already seen. According to molecular orbital theory, an s-based bonding molecular orbital has a larger overlap and lower energy than the ones based on degenerate (or almost degenerate) higher atomic angular momenta. Therefore, the stronger a_{1g} weight in the α phase is compatible with a tighter chemical bond, and so a smaller bond length and unit cell volume.

To conclude, with our embedding analysis, we showed how on-site intraorbital repulsions in the f-t_{1u} manifold accompanied by hybridization effects between the f atomic orbitals with more delocalized s and p states are responsible for the stability of the γ phase at large volumes, while the α phase is more stable at smaller volume with shorter (10%–15% difference) lattice parameters. The volume collapse transition results therefore from a tight competition between interatomic bond strength and local Coulomb repulsion.

C. Liquid hydrogen at high pressure

In this section, we present recent results on liquid hydrogen at high pressure,[78] showing the advantage of the basis set reduction in this case. We consider a MD simulation within the BO approximation, where at each step, several thousands of parameters of a JSD variational wave function have to be optimized. The use of the GEO basis set, 1 GEO in the $2s$ GTO case, and 3 GEOs in the $3s1p$ case, allows for a systematic reduction of the number of variational parameters by a factor four as compared with the primitive basis, without a sizable loss of accuracy (within 1 mHa/atom), as seen also in the case of the water molecule (Sec. III A). The reduction of the basis is achieved at the beginning of the simulation in order to start with the best possible variational wave function compatible with the small basis set chosen. The JSD wave function is composed of a Slater determinant, whose molecular orbitals are expanded in the chosen basis and that can be obtained by a DFT calculation or by a full optimization of the energy in presence of a Jastrow factor, as described in Sec. II A. A DFT calculation is first performed in the primitive basis for typical configurations at different densities and fixed hydrogen positions. After that, the contraction, namely, the determination of the initial optimal GEOs, is performed with the algorithm described in Sec. II B. Finally, the full optimization of the JSD is performed and the best JSD compatible with the GEO basis set is obtained by means of state-of-the-art optimization techniques.[32,45] Thanks to the contraction, the number of parameters to be optimized becomes affordable. Moreover, the optimization is particularly fast and reliable due to the very good initial guess obtained in this way. That makes the search for the global minimum (or at least a very good one) much simpler, being the complexity of the energy landscape reduced. For these reasons in the largest primitive basis ($6s5p1d$),[43] the statistical optimization of the molecular orbitals is not implemented, because not possible or at least very difficult, and only the Jastrow factor is optimized. In this case, however, based on smaller system calculations, we do not expect meaningful improvement in

TABLE III. Total energies per atom (in Hartree) obtained for fixed ionic configurations at different r_s with different methods: VMC, LRDMC, or RQMC; with different basis sets as described in the text. JSD+B refers to the Jastrow-Slater wave function with backflow transformation.

	$r_s = 1.44$	$r_s = 1.24$
VMC - JSD - *2s*/1GEO	−0.547 50(1)	−0.514 1(1)
VMC - JSD - *3s1p*/3GEOs	−0.553 91(1)	−0.522 46(1)
VMC - JSD - *6s5p1d* primitive	−0.554 2(1)	−0.523 0(1)
LRDMC - JSD - *2s*/1GEO	−0.552 39(1)	...
LRDMC - JSD - *3s1p*/3GEOs	−0.556 78(1)	−0.525 35(1)
VMC - JSD+B	−0.556 05(2)	−0.525 64(2)
RQMC - JSD+B	−0.557 2(1)	−0.526 38(3)

the energy by full optimization, as the determinant obtained in a large basis is essentially optimal within DFT and the LDA approximation. The results are summarized in Table III and compared with the ones obtained with other techniques, among which LRDMC and Reptation Quantum Monte Carlo (RQMC), namely, different methods to obtain the lowest variational energy compatible with the nodal surface of a given variational ansatz. LRDMC and RQMC values are obtained with standard extrapolations with the mesh size or time step, respectively, as only in this limit, they coincide if the same wave function ansatz is used in both methods.

As it is clear from Table III, by using GEOs, a small basis is enough to obtain almost converged results well below 1 mHa/atom, if we take as a reference the result of the largest primitive basis mentioned above. The best energies for the two densities (defined by r_s, such that $\frac{4}{3}\pi r_s^3 a_0^3$ is the volume per particle, a_0 being the Bohr radius) reported here are obtained with the JSD+backflow (JSD+B) ansatz, which is used in the coupled electron-ion Monte Carlo (CEIMC) calculations.[79] Here both the determinant (SD) and the Jastrow (J) are obtained with a different approach and with a different basis set. Moreover, the determinantal part SD contains also backflow correlations that are supposed to improve substantially the nodal surface of a simple Slater determinant. Nevertheless, it is quite clear that the present variational approach also in a small basis and restricted to a single determinant can provide reasonably accurate energies. Moreover, the LRDMC applied to such guiding functions is very close (within $\lesssim$1 mHa/atom) to the best RQMC results,[80] implying that the *3s1p*/3GEOs basis provides an almost optimal nodal surface.

After these successful optimizations of the basis set, we can perform MD simulations because the number of variational parameters is feasible, as at each iteration of MD, we can optimize the wave function with few steps (about 6) and compute at the final iteration the atomic forces with a reasonable computational effort. The interested reader can find more details of the MD used in our previous papers,[78,81,82] as this is outside the scope of the present work.

The results are displayed in Figs. 6 and 7 for the same two densities as in Table III, and two temperatures, 600 and 1700 K. By increasing the statistical accuracy, namely, by increasing the number L of statistical samples used for each MD step, the two basis considered ($2s$/1GEO and $3s1p$/3GEOs) extrapolate to two different energies, the difference being more than $\approx$3 mHa/atom. The extrapolation is linear, suggesting that the bias due to the finite statistical error is systematically improvable. Despite the sizable discrepancy in the $1/L \to 0$ extrapolated internal energies (see middle panels of Figs. 6 and 7), it is remarkable that the use of the small basis set does not

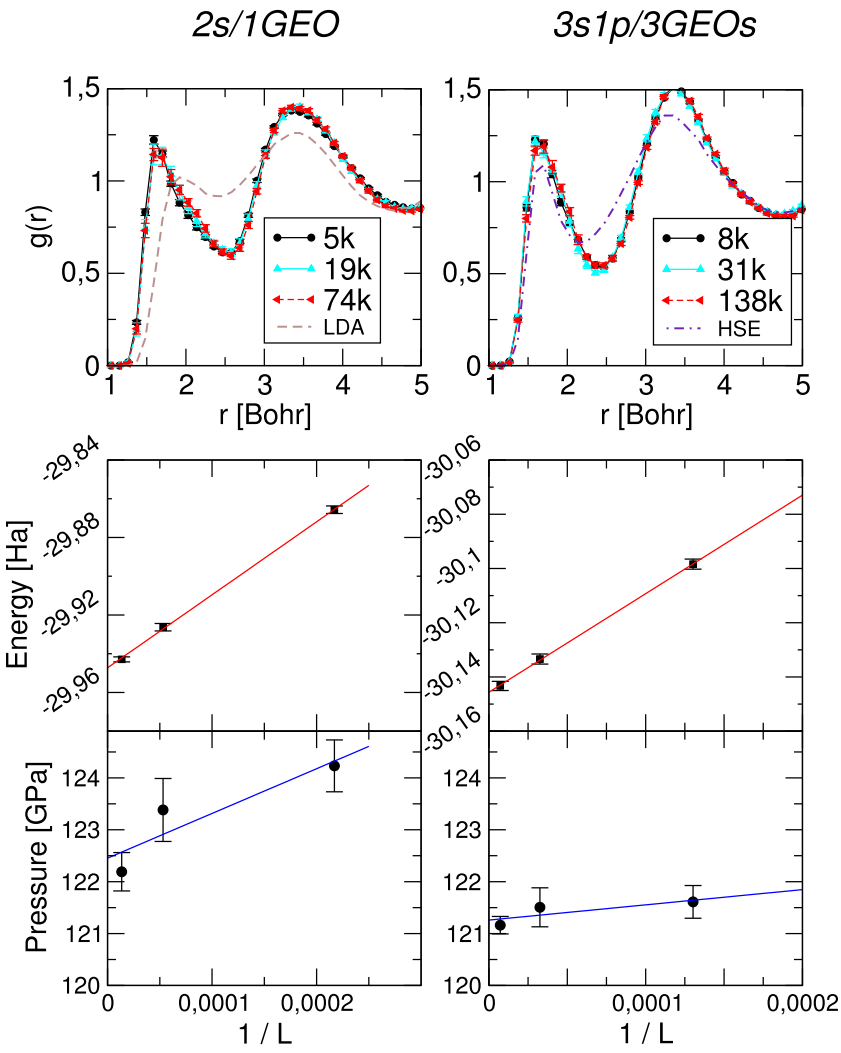

FIG. 6. Accuracy of the wave function: tests at density $r_s = 1.44$ and T = 600 K. The left panels refer to the $2s$/1GEO basis set, while the right panels to the much more accurate $3s1p$/3GEOs. Top panels: radial distribution function $g(r)$ obtained for different L (VMC sample size per MD iteration). We also plot the DFT predictions for LDA and HSE xc functionals. All the calculations are performed for 54 atoms at the Γ point. Middle panels: total energy (extensive) as a function of $1/L$. Bottom panels: pressure versus $1/L$. This quantity is rather insensitive to the statistics per iteration and the basis set.

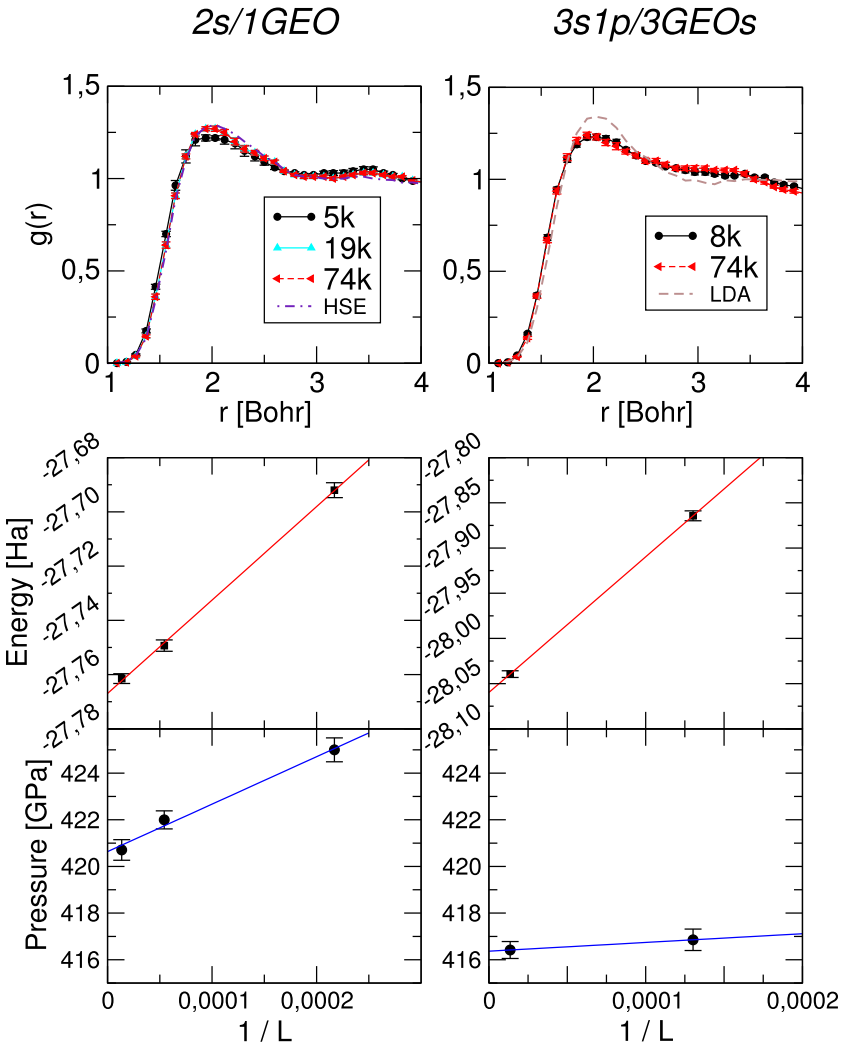

FIG. 7. Accuracy of the wave function: tests at density $r_s = 1.24$ and T = 1700 K. The left panels refer to the $2s/1$GEO basis set, while the right panels to the much more accurate $3s1p/3$GEOs. Top panels: radial distribution function $g(r)$ obtained for different L. We also plot the DFT predictions for LDA and HSE xc functional. All the calculations are performed for 54 atoms at the Γ point. Middle panels: total energy (extensive) as a function of $1/L$. The two basis extrapolate to two different energies, the difference being of ≈5 mHa/atom. Also in this case, the extrapolation is linear. Bottom panels: pressure versus $1/L$. This quantity is rather insensitive to L and the basis.

lead to any significant bias in correlation functions such as pressure (accurate within few GPa) and radial distribution functions that can be almost superposed to the largest basis set calculation, within statistical errors.

This test represents therefore a meaningful example where it is shown that by consistently optimizing a wave function in a small basis set, within a fully correlated approach, the most important correlation functions, energy differences, and derivatives are satisfactorily taken into account, opening the way for realistic large scale calculations of correlated materials.

IV. CONCLUSIONS

In this work, we have introduced a novel approach for a systematic and automatic reduction of the basis set in wave function based approaches developed on localized atomic orbitals. The method is built upon a density matrix embedding scheme, constructed by partially projecting the Slater density matrix, or the AGP geminal on a given atomic site, yielding the "geminal embedded orbitals" or GEOs. The advantage of the GEO procedure is mainly because, within our formulation, the optimal atomic natural orbitals, which diagonalize the partially projected density matrix, are obtained by solving a linear problem that has a unique, computationally feasible (scaling as the cube of the dimension of the basis), and automatic solution. The embedding devised here is also shown to be superior to the standard atomic density matrix embedding, which gives the "maximum-occupancy" natural hybrid orbitals. In the VMC framework, the method has been found very useful for the reduction of the number of variational parameters, which is otherwise prohibitive for an accurate statistical optimization, as we have seen for the water molecule and the liquid hydrogen at high pressure. The compactness of the GEO basis set also leads to remarkable physical insights into understanding the chemical bonds in molecules and solids, as is the case of cerium, presented in this work. The well known volume collapse occurring in this material is explained within this formulation as a first-order transition of electronic character, where the GEOs involving f orbitals hybridized with p states change their localization character at the transition, being broader in the γ than in the α phase, contrary to the common wisdom.

We finally comment that the present technique is not only practical to generate a more compact basis set for the Slater determinant used in HF, DFT,[1,83] and QMC calculations, but it could be extended also to other many-body approaches, by targeting the one-body density matrix of a correlated wave function, rather than the geminal in the AGP form.

Indeed, the use of a localized basis is well known to produce much better performing algorithms, and the

scheme we have introduced can be easily extended to these correlated cases and further improve the efficiency of present algorithms.[84,85]

While it is not clear that the optimal basis set found for the one-body density matrix is also optimal for the one-body basis set over which the many-body wave function is expanded, we believe that it is however a promising extension of the present technique. We remark that, in the QMC framework, whenever the dynamical correlation is treated by the Jastrow factor, the Jastrow correlated AGP ansatz recovers a substantial fraction of correlation energy in a large variety of difficult cases, where one does not need to go beyond the GEO scheme presented in this work.

Last but not least, the GEO basis set derived by the density matrix embedding scheme described in this paper can be useful to generate accurate low-energy Hamiltonians from mean-field or many-body *ab initio* calculations.

ACKNOWLEDGMENTS

One of us (S.S.) acknowledges support by MIUR-Cofin 2010. The computational resources used for this work have been partially provided by the PRACE Project No. 2012061116 and IDRIS Project No. 96493. Part of this research has used computational resources of the K computer provided by the RIKEN Advanced Institute for Computational Science through the HPCI System Research Project (Nos. hp120174 and hp140092).

[1]J. VandeVondele, M. Krack, F. Mohamed, M. Parrinello, T. Chassaing, and J. Hutter, Comput. Phys. Commun. **167**, 103 (2005).
[2]T. H. Dunning, J. Chem. Phys. **90**, 1007 (1989).
[3]K. A. Peterson and T. H. Dunning, Jr., J. Chem. Phys. **117**, 10548 (2002).
[4]K. A. Peterson and C. Puzzarini, Theor. Chem. Acc. **114**, 283 (2005).
[5]F. Weigend and R. Ahlrichs, Phys. Chem. Chem. Phys. **7**, 3297 (2005).
[6]J. Almlöf and P. R. Taylor, J. Chem. Phys. **86**, 4070 (1987).
[7]J. Almlöf, T. Helgaker, and P. R. Taylor, J. Phys. Chem. **92**, 3029 (1988).
[8]P.-O. Widmark, P.-A. Malmqvist, and B. O. Roos, Theor. Chim. Acta **77**, 291 (1990).
[9]K. Pierloot, B. Dumez, P.-O. Widmark, and B. O. Roos, Theor. Chim. Acta **90**, 87 (1995).
[10]B. O. Roos, R. Lindh, P.-A. Malmqvist, V. Veryazov, and P.-O. Widmark, J. Phys. Chem. A **108**, 2851 (2004).
[11]F. R. Petruzielo, J. Toulouse, and C. J. Umrigar, J. Chem. Phys. **132**, 094109 (2010).
[12]F. R. Petruzielo, J. Toulouse, and C. J. Umrigar, J. Chem. Phys. **134**, 064104 (2011).
[13]P.-O. Löwdin, Phys. Rev. **97**, 1474 (1955).
[14]J. P. Foster and F. Weinhold, J. Am. Chem. Soc. **102**, 7211 (1980).
[15]A. E. Reed, R. B. Weinstock, and F. Weinhold, J. Chem. Phys. **83**, 735 (1985).
[16]R. F. W. Bader, T. T. Nguyen-Dang, and Y. Tal, Rep. Prog. Phys. **44**, 893 (1981).
[17]J. Cioslowski, Int. J. Quantum Chem. **38**, 015 (1990).
[18]J. Cioslowski and A. Liashenko, J. Chem. Phys. **108**, 4405 (1998).
[19]I. Mayer, Chem. Phys. Lett. **242**, 499 (1995).
[20]M. S. Lee and M. Head-Gordon, Int. J. Quantum Chem. **76**, 169 (2000).
[21]D. N. Laikov, Int. J. Quantum Chem. **111**, 2851 (2011).
[22]B. Lange, C. Freysoldt, and J. Neugebauer, Phys. Rev. B **84**, 085101 (2011).
[23]G. Knizia, J. Chem. Theory Comput. **9**, 4834 (2013).
[24]A. C. West, M. W. Schmidt, M. S. Gordon, and K. Ruedenberg, J. Chem. Phys. **139**, 234107 (2013).
[25]M. Casula, C. Attaccalite, and S. Sorella, J. Chem. Phys. **121**, 7110 (2004).
[26]N. D. Drummond, M. D. Towler, and R. J. Needs, Phys. Rev. B **70**, 235119 (2004).
[27]T. Kato, Commun. Pure Appl. Math. **10**, 151 (1957).
[28]F. R. Petruzielo, J. Toulouse, and C. J. Umrigar, J. Chem. Phys. **136**, 124116 (2012).
[29]M. Casula and S. Sorella, J. Chem. Phys. **119**, 6500 (2003).
[30]M. Bajdich, L. Mitas, G. Drobný, L. K. Wagner, and K. E. Schmidt, Phys. Rev. Lett. **96**, 130201 (2006).
[31]M. Bajdich, L. Mitas, L. K. Wagner, and K. E. Schmidt, Phys. Rev. B **77**, 115112 (2008).
[32]C. J. Umrigar, J. Toulouse, C. Filippi, S. Sorella, and R. G. Hennig, Phys. Rev. Lett. **98**, 110201 (2006).
[33]J. Toulouse and C. J. Umrigar, J. Chem. Phys. **128**, 174101 (2008).
[34]C. Attaccalite and S. Sorella, Phys. Rev. Lett. **100**, 114501 (2008).
[35]J. Von Neumann, *Mathematische Grundlagen der Quantenmechanik* (Springer, Berlin, 1932).
[36]K. A. Hallberg, Adv. Phys. **55**, 477 (2006).
[37]S. R. White, Phys. Rev. Lett. **69**, 2863 (1992).
[38]G. Knizia and G. K.-L. Chan, Phys. Rev. Lett. **109**, 186404 (2012).
[39]G. Knizia and G. K.-L. Chan, J. Chem. Theory Comput. **9**, 1428 (2013).
[40]I. W. Bulik, G. E. Scuseria, and J. Dukelsky, Phys. Rev. B **89**, 035140 (2014).
[41]I. W. Bulik, W. Chen, and G. E. Scuseria, J. Chem. Phys. **141**, 054113 (2014).
[42]Q. Sun and G. K.-L. Chan, J. Chem. Theory Comput. **10**, 3784 (2014).
[43]M. Burkatzki, C. Filippi, and M. Dolg, J. Chem. Phys. **126**, 234105 (2007).
[44]M. Dolg, private communication (2013).
[45]S. Sorella, M. Casula, and D. Rocca, J. Chem. Phys. **127**, 014105 (2007).
[46]M. Barborini, S. Sorella, and L. Guidoni, J. Chem. Theory Comput. **8**, 1260 (2012).
[47]S. Sorella, M. Casula, L. Spanu, and A. Dal Corso, Phys. Rev. B **83**, 075119 (2011).
[48]M. Marchi, S. Azadi, and S. Sorella, Phys. Rev. Lett. **107**, 086807 (2011).
[49]M. Casula and S. Sorella, Phys. Rev. B **88**, 155125 (2013).
[50]E. Coccia, O. Chernomor, M. Barborini, S. Sorella, and L. Guidoni, J. Chem. Theory Comput. **8**, 1952 (2012).
[51]D. Bohm and D. Pines, Phys. Rev. **92**, 609 (1953).
[52]A. J. Williamson, S. D. Kenny, G. Rajagopal, A. J. James, R. J. Needs, L. M. Fraser, W. M. C. Foulkes, and P. Maccullum, Phys. Rev. B **53**, 9640 (1996).
[53]P. López Ríos, P. Seth, N. D. Drummond, and R. J. Needs, Phys. Rev. E **86**, 036703 (2012).
[54]S. Sorella, TurboRVB, 2010.
[55]Here, the matrix λ^{AGP} is a diagonal one with matrix elements $\lambda_k^{\mathrm{AGP}}\delta_{k,k'}$.
[56]This linear problem corresponds to a generalized eigensystem equation of the type $ABx = \lambda x$ with $A = \lambda s \lambda^\dagger$ a symmetric matrix and $B = s$ a symmetric and positive definite one, x and λ being the eigenvector and the corresponding eigenvalue, respectively.
[57]A. Lüchow and R. F. Fink, J. Chem. Phys. **113**, 8457 (2000).
[58]D. Feller, C. M. Boyle, and E. R. Davidson, J. Chem. Phys. **86**, 3424 (1987).
[59]N. A. Benedek, I. K. Snook, M. D. Towler, and R. J. Needs, J. Chem. Phys. **125**, 104302 (2006).
[60]F. Sterpone, L. Spanu, L. Ferraro, S. Sorella, and L. Guidoni, J. Chem. Theory Comput. **4**, 1428 (2008).
[61]M. J. Gillan, F. R. Manby, M. D. Towler, and D. Alfé, J. Chem. Phys. **136**, 244105 (2012).
[62]M. Dagrada, M. Casula, A. M. Saitta, S. Sorella, and F. Mauri, J. Chem. Theory Comput. **10**, 1980 (2014).
[63]M. Marchi, S. Azadi, M. Casula, and S. Sorella, J. Chem. Phys. **131**, 154116 (2009).
[64]M. Burkatzki, C. Filippi, and M. Dolg, J. Chem. Phys. **126**, 234105 (2007).
[65]A. Zen, Y. Luo, S. Sorella, and L. Guidoni, J. Chem. Theory Comput. **9**, 4332 (2013).
[66]M. Casula, C. Filippi, and S. Sorella, Phys. Rev. Lett. **95**, 100201 (2005).
[67]M. Casula, S. Moroni, S. Sorella, and C. Filippi, J. Chem. Phys. **132**, 154113 (2010).
[68]A. Svane, Phys. Rev. Lett. **72**, 1248 (1994).
[69]M. Casadei, X. Ren, P. Rinke, A. Rubio, and M. Scheffler, Phys. Rev. Lett. **109**, 146402 (2012).
[70]N. Lanatà, Y.-X. Yao, C.-Z. Wang, K.-M. Ho, J. Schmalian, K. Haule, and G. Kotliar, Phys. Rev. Lett. **111**, 196801 (2013).
[71]M.-F. Tian, H.-F. Song, H.-F. Liu, C. Wang, Z. Fang, and X. Dai, Phys. Rev. B **91**, 125148 (2015).
[72]B. Amadon and A. Gerossier, Phys. Rev. B **91**, 161103 (2015).
[73]F. Decremps, L. Belhadi, D. L. Farber, K. T. Moore, F. Occelli, M. Gauthier, A. Polian, D. Antonangeli, C. M. Aracne-Ruddle, and B. Amadon, Phys. Rev. Lett. **106**, 065701 (2011).
[74]J. W. Allen and R. M. Martin, Phys. Rev. Lett. **49**, 1106 (1982).
[75]A. K. McMahan, K. Held, and R. T. Scalettar, Phys. Rev. B **67**, 075108 (2003).
[76]B. Amadon, S. Biermann, A. Georges, and F. Aryasetiawan, Phys. Rev. Lett. **96**, 066402 (2006).

[77]N. Devaux, M. Casula, F. Decremps, and S. Sorella, Phys. Rev. B **91**, 08110(R) (2015).
[78]G. Mazzola and S. Sorella, Phys. Rev. Lett. **114**, 105701 (2015).
[79]M. A. Morales, C. Pierleoni, E. Schwegler, and D. M. Ceperley, Proc. Natl. Acad. Sci. U. S. A. **107**, 12799 (2010).
[80]S. Baroni and S. Moroni, Phys. Rev. Lett. **82**, 4745 (1999).
[81]Y. Luo, A. Zen, and S. Sorella, J. Chem. Phys. **141**, 194112 (2014).
[82]G. Mazzola, S. Yunoki, and S. Sorella, Nat. Commun. **5**, 3487 (2014).
[83]J. M. Soler, E. Artacho, J. D. Gale, A. Garcia, J. Junquera, P. Ordejon, and D. Sanchez-Portal, J. Phys.: Condens. Matter **14**, 2745 (2002).
[84]A. Marini, C. Hogan, M. Grüning, and D. Varsano, Comput. Phys. Commun. **180**, 1392 (2009).
[85]P. Giannozzi, S. Baroni, N. Bonini, M. Calandra, R. Car, C. Cavazzoni, D. Ceresoli, G. L. Chiarotti, M. Cococcioni, I. Dabo, A. Dal Corso, S. de Gironcoli, S. Fabris, G. Fratesi, R. Gebauer, U. Gerstmann, C. Gougoussis, A. Kokalj, M. Lazzeri, L. Martin-Samos, N. Marzari, F. Mauri, R. Mazzarello, S. Paolini, A. Pasquarello, L. Paulatto, C. Sbraccia, S. Scandolo, G. Sclauzero, A. P. Seitsonen, A. Smogunov, P. Umari, and R. M. Wentzcovitch, J. Phys.: Condens. Matter **21**, 395502 (2009).